A&A 432, 619–632 (2005)
DOI: 10.1051/0004-6361:20041248

Astronomy & Astrophysics

On the nature of pre-main sequence candidate stars in the Large Magellanic Cloud⋆

W. J. de Wit[1,⋆⋆], J. P. Beaulieu[2], H. J. G. L. M. Lamers[3,4], C. Coutures[5], and G. Meeus[6]

[1] INAF - Osservatorio Astrofisico di Arcetri, Largo E. Fermi 5, 50125 Florence, Italy
e-mail: dewit@obs.ujf-grenoble.fr
[2] Institut d'Astrophysique de Paris, 98 bis boulevard Arago, 75014 Paris, France
[3] Astronomical Institute, University of Utrecht, Princetonplein 5, 3584 CC, Utrecht, The Netherlands
[4] SRON Laboratory for Space Research, Sorbonnelaan 2, 3584 CA, Utrecht, The Netherlands
[5] CEA, DSM, DAPNIA, Centre d'Études de Saclay, 91191 Gif-sur-Yvette Cedex, France
[6] Astrophysikalisches Institut Potsdam, An der Sternwarte 16, 14482 Potsdam, Germany

Received 22 April 2004 / Accepted 7 November 2004

Abstract. We investigate a sample of 18 Large Magellanic Cloud Herbig Ae/Be candidate stars looking at their (1) spectral types (2) brightness variability mechanism and (3) near infra-red JHK emission. We find that the majority of the target stars have Hα emission, are of spectral type early- to mid-B and lack strong JHK excess emission. Their Balmer decrements are found to be similar to that of Galactic Be stars in general. Their erratic brightness variability is evaluated by using the observed optical color excess and the color gradient from the light curves and is subsequently interpreted as being due to variable dust obscuration or variable bf-ff emission from circumstellar ionized gas. For approximately half of the target stars in our sample the type of variability seems to be dissimilar to the mechanism involving bound-free and free-free emission, but could be interpreted as caused by variable dust obscuration, as we have proposed in earlier studies. It is therefore suggested that they are pre-main sequence objects, despite the fact that they nearly all lack thermal dust emission in the near infra-red; mid/far infra-red observations for these objects are warranted. One star is observed to have JHK excess emission and an inspection of its 7.5 year MACHO light curve confirms its erratic photometric behavior. The object displays deep photometric minima with a quasi-period of 191.3 days, as generally seen in the Galactic pre-main sequence subgroup of the UX Orionis stars.

Key words. stars: formation – stars: emission-line, Be – stars: variables: general – stars: pre-main sequence – galaxies: Magellanic Clouds

1. Introduction

Extragalactic pre-main sequence (PMS) stars can provide valuable clues for an understanding of the processes that govern star formation at various metallicities. For example, the abundance of dust and cooling molecules may effect the efficiency of ambipolar diffusion and cloud collapse during the initial formation stages and the survival time of the circumstellar accretion disk later on. Characteristic scales of these processes are therefore likely to vary with metallicity. In particular, a *short* formation time scale of stars at lower metallicity could be inferred from the many blue globular sized star clusters in the Large Magellanic Cloud (LMC). To form such clusters, large amounts of gas and a quick collapse are required (see Hunter 1997).

Magellanic Cloud PMS objects offer the opportunity to study in detail the formation rate and evolution of individual young stars at different metallicities. Seven LMC PMS candidate stars were discovered by Beaulieu et al. (1996). These objects were selected because they exhibit a peculiar type of photometric variability with a time scale typically observed among Galactic HAeBe stars, as revealed by their light curves obtained by the EROS collaboration (e.g. Aubourg et al. 1993). In a follow-up study (Lamers et al. 1999, hereafter LBD), other common HAeBe features corroborate the conjecture that the objects are PMS stars: (1) similar spectral type (2) similar Hα emission (3) similar luminosity class (4) an inferred (unresolved) reflection nebula and (5) a location in or near H II regions in the LMC bar. Therefore they proposed to use the name **E**ros **L**MC **H**AeBe **C**andidates or ELHC, which we use throughout this paper. On larger scales, evidence for star formation in this particular region of the LMC bar was provided by the IRAS satellite. The ELHCs are located in or near the rim of a large 60 μm emission region (de Wit et al. 2002, hereafter Paper I), evidence of a young nature for the ELHCs.

Meanwhile, fourteen similar peculiar photometric variables were identified and used to enlarge the number of HAeBe candidate stars in the LMC to 21 objects (Paper I). Nearly all the objects (18/21) are located in a strip of 100 by 450 pc in the bar, following the general direction of the 60 μm emission.

⋆ Based on observations collected at ESO, La Silla.
⋆⋆ Now at Laboratoire d'Astrophysique de Grenoble.

To the south, the strip is bounded by the H II region N 120 and the OB association LH 42; seven ELHCs are located in this complex area (see Laval et al. 1992). To the north, the strip is bounded by the H II region N 119 and the OB association LH 41. The strip is filled with filamentary ionized gas and extended H II emission regions. De Wit et al. (2001) showed statistically that the odds of being located in small clusters or near other Hα emitters are larger for the HAeBe candidate stars than for stars of the same spectral type and luminosity class. In all, the individual and global characteristics of the ELHCs strengthen the initial proposition made by Beaulieu et al. (1996).

The most notable difference between the ELHCs and Galactic HAeBe stars is their luminosity. The ELHCs have luminosities generally higher, which could be indicative of a shorter formation time scale. Compared to the time scales appropriate for the canonical Galactic mass accretion rate of $10^{-5}\ M_{\odot}\,\mathrm{yr}^{-1}$ (Palla & Stahler 1993), the ELHCs could have been formed ten times faster. This supports the notion of the quick collapse phase for the blue globular sized clusters. A high present-day mass accretion rate in the LMC is also inferred from the Balmer continuum and Hα emission of T Tauri stars located within a distance of 15 pc from SN1987A (Panagia et al. 2000; Romaniello et al. 2004). On the contrary, no difference in star formation between the Galaxy and the LMC is obvious in the 30 Dor region (Brandner et al. 2001), as derived from a comparison of infra-red (IR) properties of Class I protostars detected in the region's nebular filaments.

However, it has not been conclusively proven that the ELHCs are in fact HAeBe stars. A number of the above listed stellar characteristics of the ELHCs are common to classical Be stars as well, i.e. (Post) Main Sequence B-type stars of luminosity class III-V, which show or have shown Balmer line emission. LBD noted that if the ELHC objects are not PMS stars but rather classical Be stars, then their observed variability is a new and rarely observed type of variability of classical Be stars. Indeed, more recently Keller et al. (2002) presented a large sample of 1279 blue variable LMC objects, including 4 ELHC stars presented by LBD, based on the seven years of observations by the MACHO collaboration. These objects show an impressive variety in their photometric variability. The authors favor the interpretation that the variability of these stars is related to the Be star phenomenon. The decisive argument for a young nature of the ELHCs can be provided by circumstellar (CS) IR excess. HAeBe stars have strong CS IR excess emission due to heated dust (Waters & Waelkens 1998), whereas classical Be star have a small IR excess caused by Bremsstrahlung originating in their CS disks.

The purpose of this paper is to combine spectral and IR diagnostics of the ELHC sample of 21 objects with the objective to clarify the nature of the ELHC stars. For this we present an optical analysis of 10 new candidates in the form of spectra in Sect. 2. The spectra of the first seven ELHCs were presented in LBD. IR photometry is the subject of Sect. 3. In Sect. 4, we perform an analysis of the optical ELHC light curves. Discussion of the lack of NIR excess and the mechanism causing the optical variability is presented in Sect. 5. We conclude in Sect. 6.

2. Presentation of the optical spectra

2.1. Observations and reduction

During different observation runs we have secured low and medium resolution spectra for 10 new LMC HAeBe candidate stars. These objects were presented in Paper I. The spectra were obtained partly with EFOSC2 on the 3.6 m Telescope and partly with DFOSC on the Danish 1.5 m Telescope at the ESO La Silla facility. We used the EFOSC2 instrument with grism #6 (wavelength range: 3860–8070 Å) and the higher resolution grism #7 (wavelength range: 3270–5240 Å) in order to cover the most important classification lines and Hα. The DFOSC spectra were taken with the grism #7 (wavelength range: 3850–6750 Å). Different slit widths were used depending on the seeing during the night. The complete log of the observations is given in Table 1. The data were processed with the MIDAS 97NOV package, using the LONG context. Wavelength calibration was done on He Ne Ar arc line spectrum for the DFOSC spectra and He Ne arc line spectrum for EFOSC spectra. Additional wavelength calibration was performed by using the most prominent sky lines of O I.

2.2. General description of the spectra

The ELHCs were initially selected on their irregular brightness variability and color, i.e. $(B_{\rm E} - R_{\rm E}) < 0.5$, where $B_{\rm E}$ and $R_{\rm E}$ are the EROS broad band filters. The color allows selection of stars earlier than F-type, accounting for modest extinction towards the LMC. Two spectral properties appear to be common to ELHCs: (1) nearly all stars are B-type, despite the adopted color limit and (2) all stars have Balmer line emission, although this was not a selection criterion. It suggests that A-type stars are less variable or absent (see also Paper I) and that Balmer emission and variability are closely connected.

A classification scheme for B-type stars has been constructed by Didelon (1982). The scheme uses the equivalent width (EW) of the classifying lines of H I, He I, He II, C III/O II and other indicative metallic lines such as Mg II, the ionized species of Si and N II/N III as a function of B spectral type and luminosity class. The spectral resolution allows us to classify the stars primarily on the EW of the He I lines. We constrain the classification by the presence (or absence) of the C III/O II 4650 Å blend and the He II lines, which is the prime difference between B-type and O-type stars. He II lines are also observed in low-mass PMS stars, but scarcely, if at all, in Herbig AeBe stars (Hamann & Persson 1992). Due to their emission character we do not use the Balmer lines. The spectra discussed in this section are presented in Fig. 1. We display the important wavelength interval between 3900 Å and 5000 Å, with the classification lines and blends indicated.

For some stars the S/N ratio was high enough to detect metallic lines and thus constrain the spectral types. The spectral type of other objects could not be well determined from the observed EW of the indicative lines. Therefore we allowed for considerable uncertainty, depending on the S/N, in the spectral type determination. In Table 1, the results of the spectral

Table 1. Overview of the spectroscopic observations and the result of the spectral type analysis (Col. 4) as described in Sect. 2.3. The spectra themselves are displayed in Fig. 1.

ELHC	RA(2000)	Dec(2000)	Sp. type	Date	Instrument	Range (Å)	Exp (s)	$\langle S/N \rangle$	R
8	05 17 17.7	–69 33 34.2	B2-4 III/IV	07–03–2000	EFOSC2 3.6 m	3900–8000	300	80	400
				07–03–2000		3250–5200	1200	100	800
10[1]	05 19 48.3	–69 39 09.6	F2-5 I/II	08–01–1998	DFOSC 1.5 m-Dan	3850–6750	2418	70	1000
11	05 18 36.2	–69 35 60.0	B1 III	07–03–2000	EFOSC2 3.6 m	3250–5200	1200	100	400
12	05 18 50.0	–69 35 21.2	early B	06–01–1998	EFOSC 3.6 m	3850–8050	300	30	450
				06–01–1998		3260–5230	900	15	900
13	05 18 54.9	–69 36 35.8	B1-2 III/V	09–03–2000	EFOSC2 3.6 m	3900–8000	300	70	400
				09–03–2000		3250–5200	1200	80	800
14	05 19 54.9	–69 42 04.0	B1 III/IV	09–03–2000	EFOSC2 3.6 m	3900–8000	300	70	400
				09–03–2000		3250–5200	1200	80	800
16	05 20 28.0	–69 35 36.5	B1-4 III/V	06–01–1998	EFOSC 3.6 m	3850–8050	300	70	450
19	05 17 11.8	–69 25 54.0	B1-5 III/V	06–01–1998	EFOSC 3.6 m	3850–8050	300	40	450
				06–01–1998		3260–5230	900	50	900
20	05 16 22.5	–69 20 19.3	B1-5 III/V	06–01–1998	EFOSC 3.6 m	3850–8050	300	60	450
21	05 19 45.0	–69 26 16.4	B1-2 III/V	08–01–1998	DFOSC 1.5 m-Dan	3850–6750	1800	45	1000

1. The star is also known as [BE74] 561.

analysis are listed in Col. 4. The exact considerations for each star are given in the following section.

2.3. Notes on individual objects

ELHC 8

For ELHC 8 we have obtained low and medium resolution spectra. Hα is in emission with a *FWHM* 13.6 and an equivalent width of 34.0 Å. Both Hβ as well as Hγ have emission components with a *FWHM* of 4.6 Å and 3.2 Å respectively. One other emission feature is detected at Fe II λ5169. The spectrum shows the following metal lines: C II at λ4267 and Si III at $\lambda\lambda$4567, 4574 and 4819. A strong N II at 4237 Å was detected. The observed lines indicate a star of B0 to B2 type. The *EW* of the He I lines indicates a LC III–V. The absence of He II λ4685 then gives a spectral type of B2/4 III–IV. The lack of any visible O II and Mg II lines and the presence of C II, limits the spectral type to B2III-IV.

ELHC 10

ELHC 10 is the reddest star in our sample with $(B-V) = 0.3$, and also the brightest with an estimated $M_V = -4.7^m$. Its spectrum displays Hα emission with an *EW* of 23 Å. Unlike the other ELHCs this star is not an early B star, but an F star. For this reason, its spectrum in Fig. 1 is displayed on the bottom row, set apart from the other ELHCs. We determined its spectral type, using the classification method for F–K stars developed by Malyuto & Schmidt-Kaler (1997) based on temperature-sensitive wavelength regions. The stellar spectrum is most compatible with an early F star of giant or supergiant luminosity class. We constrained the spectral type further by fitting spectral type sensitive wavelength intervals defined by Malyuto & Schmidt-Kaler with standard stellar spectra from Jacoby (1984). We systematically obtained the best fit for an F5I star in all wavelength intervals. The measured V-magnitude of the star however indicates a luminosity that is smaller than typical for a star of luminosity class I. ELHC 10 cannot be reddened much, as its color of $(B-V) = 0.30$ is appropriate for early F-type stars. We estimate the star to be F2/5 I–II.

ELHC 11

For this star we obtained a medium resolution spectrum from 3300 Å to 5200 Å. On the CCD frame, a spectrum of an F type star is found close to the target spectrum (<2″). This secondary star in not resolved on the EROS images. The target spectrum has a high average signal to noise ratio of 100. Hβ has a weak emission component. No other emission features are evident. For the classification of ELHC 11 we were able to measure many important lines in addition to the 4650 Å blend, including Si II/Si III/Si IV, O II and N II. C II was absent, which limits the star to earlier than B2 type. Combining this with the absence of He II we can determine the spectral type accurately as a B1 III star. The *EW* of ten lines are compatible with this spectral type. The He I line at 4390 Å is however much stronger than expected.

ELHC 12

The S/N of both spectra are low. The star has Hα and Hβ in emission. The only other features detectable are Hγ, Hδ and some He I lines. Therefore we classify the star as early B type with considerable uncertainty.

ELHC 13

Hα is in emission with a *FWHM* of 14.4 Å and an *EW* of 35.4 Å. Both Hβ and Hγ have emission components on top of the photospheric component. The presence of Si III at λ4552 constrains the spectral type to earlier than B4, while the

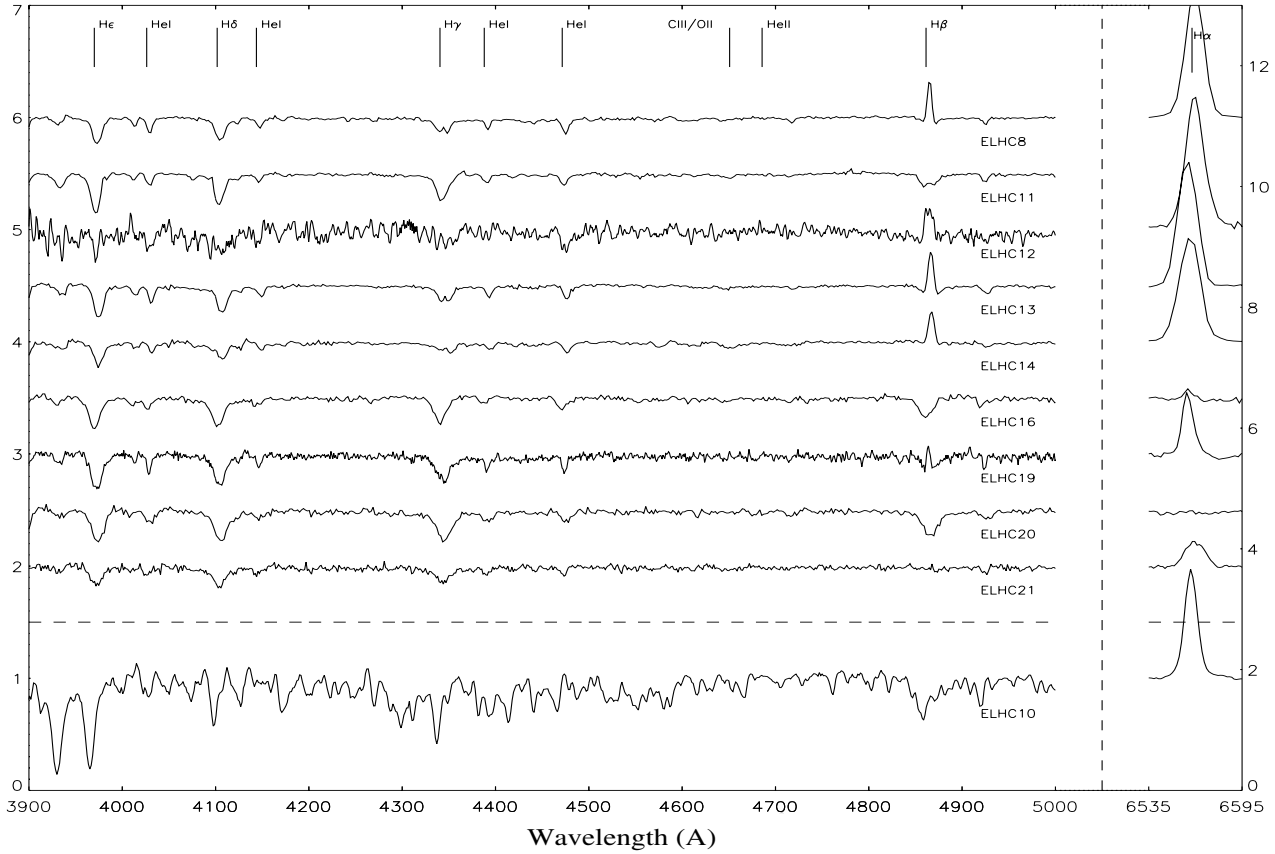

Fig. 1. The spectra of the target stars in the interval 3900 Å–5000 Å and the wavelength region at Hα . Each spectrum is indicated by its ELHC number. The lines used for classification are indicated. The bottom spectrum shows the F-type star ELHC 10 and is set apart to mark the difference from the other ELHCs.

absence of He II λ4685 makes the star later than B1. The *EW* of the He I lines are large, and compatible with B1–B4 III–V. Finally, the presence of C II/O III λ4650 blend gives a B1–B2 spectral type.

ELHC 14

Hα is in emission, with *FWHM* of 15.9 Å and an *EW* of 33.0 Å. Hβ, Hγ and Hδ have emission components on top of the photospheric component. The C III/O II λ4650 blend is very strong and very wide (*FWHM* 21 Å), due to the contributions of O II at 4641 Å and C III at 4650 Å. Strong absorption components can be found at λ4574 (Si III) and at λ4714 (O II), λ5009 (N II), where at this wavelength the He I line blends in. From the absence of He II at 4685 Å and the rapid decrease of C III among early B-type stars, we conclude that this star is a B1 star of luminosity class III–IV.

ELHC 16

For ELHC 16 only a low resolution spectrum was obtained. For its spectral type determination we used primarily the He I lines. Only Hα is filled in, no other emission lines are apparent. In the red part the spectrum is contaminated by a close companion. The C III/O II blend is not detectable. The *EW* of the He I lines at $\lambda\lambda$4026, 4143, 4387, 4473 are compatible with a spectral of B1–4 III/V.

ELHC 19

The S/N of the spectrum of ELHC 19 is ∼35 for the red part near Hα, but quickly increases towards the blue. The empirically-estimated minimum *EW* for detection is 0.3 Å at 4500 Å. One can constrain the spectral type from the non-detection of Mg II to be earlier than B5, while the non-detection of He II indicates that the star should be later than B0. The 4650 Å blend is not detected. The He I lines are particularly narrow and from their HWHM we deduce a $v \sin i \lesssim 200 \pm 20\,\mathrm{km\,s^{-1}}$. In contrast, the higher Balmer absorption lines are best fitted with model profiles which are broadened, corresponding to a rotational velocity of $v_{\rm rot} = 400\,\mathrm{km\,s^{-1}}$. This is shown more clearly in Fig. 2. The figure compares part of the Balmer series with synthetic profiles (dashed lines) computed with SYNSPEC (Hubeny et al. 1994). The dashed lines indicate $v_{\rm rad} \pm v \sin i$ determined from the He I lines. Among early type rapid rotators, narrow He I absorption profiles and Balmer absorption profiles with broad wings can be understood in terms of an inclination effect. The Balmer lines are more sensitive to the linear Stark effect than the He I lines. The Stark effect is large at the pole of a rapid rotator due to the higher effective gravity and can therefore produce extended wings in the Balmer profiles (see Slettebak 1949). On the other hand, the He I profiles are broadened mainly due to the Doppler effect corresponding to the low $v \sin i$, viewed under a small inclination by the observer. Therefore it is believed that rapid rotators, like classical Be stars, that show these spectral features are observed "pole-on". ELHC 19 could be displaying an out flowing wind, which one can deduce from the blue-shifted emission

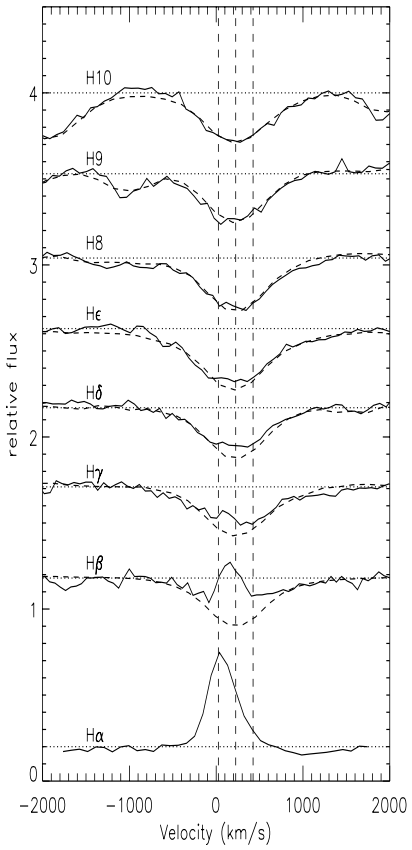

Fig. 2. The observed Balmer series of ELHC 19 (full lines) compared to predicted Balmer lines (dashed lines) for $T_{\rm eff}$ = 22 000 K, $\log(g)$ = 4.0 atmosphere (SYNSPEC). Note the flux increase in the blue wing of the Hγ to Hα line. We applied a convolution corresponding to a rotational velocity of $v_{\rm rot}$ = 400 km s^{-1} to the model lines. Zero radial velocity in the figure corresponds to the wavelength of the Balmer lines in the earth's rest frame. The vertical line at v = 225 km s^{-1} indicates the velocity offset from the rest wavelength for the higher Balmer lines (Hδ to H10). The adjacent lines indicate the 225 km s^{-1} ± $v \sin i$ determined from the HWHM of the He I lines.

components in the lower Balmer lines in Fig. 2. It seems less likely that the blue-shifted emission is due to the V/R effect due to a one-armed spiral in the gaseous CS disk of classical Be stars (Hanuschik et al. 1995; Okazaki 1991). V/R emission peaks are generally not observed at velocities close to $v_{\rm rad} \pm v \sin i$, as is the case for the Hα line of ELHC 19. Instead, the V/R emission peaks are rather at moderate offsets from the peculiar velocity of the Be star (see Hanuschik et al. 1996). We see thus that the Balmer and He I profiles of ELHC 19 can be understood in terms of a rapid rotator, viewed at a low inclination, with evidence for a stellar wind. The *EW* of the most important He I lines are compatible with a B1–B5 star.

ELHC 20

For ELHC 20 we have obtained only a low resolution spectrum, which inhibits a good classification. We classify this star on the *EW* of the He I lines and the 4650 Å blend. The Hα profile is filled by an emission component. The 4650 Å blend is not detected. The He I lines are particularly strong, indicative of luminosity class III–V. The *EW* of the most important He I lines are compatible with a B1–B5 star.

ELHC 21

For ELHC 21 we have obtained a low resolution spectra. Hα is in emission with a *FWHM* of 14.5 Å and Hβ is filled with emission. The other Balmer lines up to H 8 all seem to have an emission core in their profile. The empirically estimated minimum *EW* for detection is 0.30 Å at λ4500. It could be that the 4650 Å blend is present, but very weak. The He I λ4120 line is present and has an *EW* of 0.25 ± 0.1 Å. The *EW* of this line in B stars is small, and decreases to later spectral type. Considering the S/N of the spectrum of ELHC 21, its presence argues for a quite early spectral type. An unidentified line is present at 5646 Å. Metal lines other then He I do not seem present at this resolution and S/N, except a very weak 4650 Å blend and possibly the Si III line at λ4552. He II is absent. These characteristics constrain the star to be a B1–2 III–V star. The *EW* of the 4 most important He I classification lines are compatible with this spectral type. Nebular lines of [O III] λ5006.8 in the rest frame of ELHC 21 are detected in the background sky. The origin could be the SNR in which ELHC 21 is located.

Summarizing, the spectra show that nearly all ELHCs are mid to early B-type stars with estimated luminosity classes between III and V, with ELHC 10 (spectral type F) as exception. The results of the classification are summarized in Col. 4 of Table 1.

2.4. Balmer decrement and forbidden line emission

We evaluate the intensity ratios of Hα, Hβ and Hγ, i.e. the Balmer decrements D_{34} and D_{54} for those ELHCs with the strongest optical emission lines.

We measure the decrement following the recipe of Dachs et al. (1990), where the observed emission equivalent width is corrected for the underlying photospheric absorption and the local continuum flux. The photospheric absorption is estimated using the derived spectral types and atmosphere models using SYNSPEC (Hubeny et al. 1994). The continuum fluxes at the three Balmer lines were adopted as the same for all stars, considering that the optical continuum is already well approximated by the Rayleigh-Jeans law and therefore not very sensitive to the stellar parameters. We took the values $F_{\rm cont}({\rm H}\gamma)/F_{\rm cont}({\rm H}\beta)$ = 1.43 and $F_{\rm cont}({\rm H}\alpha)/F_{\rm cont}({\rm H}\beta)$ = 0.35 from Štefl et al. (2003). For six ELHCs the Balmer decrement in both D_{34} and D_{54} could be measured to a reasonable accuracy, while for the other stars we lacked either spectroscopic information on the Hα emission line, or the spectra were of low S/N.

In Fig. 3 we compare the obtained decrements with the ones observed of Galactic classical Be stars indicated by the large dashed square (Dachs et al. 1990) and Herbig Be stars (open circles). The decrements of the 8 Herbig Be stars were measured from the spectra by Hernández et al. (2004)[1], and by computing SYNSPEC spectra according to the spectral types given by these authors. The Herbig Be stars range in spectral type from B 1 (LkHa 118) to B 6 (HD 259431). The large "B"

[1] From `http://cfa-www.harvard.edu/youngstars/jhernand/haebe/`

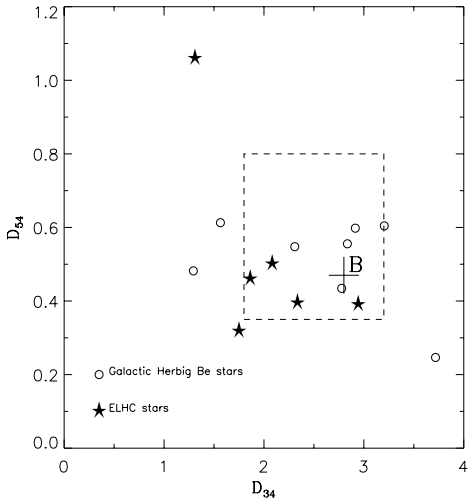

Fig. 3. The Balmer decrement for Herbig Be and classical Be stars compared to the LMC PMS candidate stars. The Hγ to Hβ Balmer decrement is plotted against the Hα to Hβ Balmer decrement. Case B recombination is indicated by the cross and the "B". The large dashed square indicates the region occupied by classical Be stars with $EW(\mathrm{H}\alpha) \gtrsim 25$ Å (Dachs et al. 1990). The open circles are Galactic Herbig Be stars, and the asterisks are ELHC stars. Herbig Be, classical Be and ELHC stars occupy practically the same region in this diagram.

in Fig. 3 indicates the expected values for the decrements when the gas would be under case B conditions.

The Galactic Herbig Be stars are located in the same region in Fig. 3 as the classical Be stars, indicating a similar state of the CS gas. The Balmer decrement of the 6 ELHC stars do not show a different distribution from that of Galactic Be or Herbig Be stars, again indicating that the electron density and temperature of the CS gas can be very similar near Be-type stars in general.

Apart from the Balmer line emission, no other emission lines were detected, except for permitted Fe II emission in ELHC 8. In particular no forbidden line emission was detected. The presence of forbidden line emission of HAeBe stars was mentioned in Finkenzeller & Mundt (1984) and more systematically studied by Böhm & Catala (1994) and Böhm & Hirth (1997). In a recent spectroscopic analysis of 131 HAeBe stars by Vieira et al. (2003) it is shown that nearly 50% of the stars have [O I] and/or [S II] emission, especially among the B type stars of their sample. The obtained S/N of the spectra of the ELHCs allow 3σ detections for lines with EW of ∼1 Å for the lowest S/N and ∼0.5 Å for the highest. The large majority of the HAeBe stars from Böhm & Catala (1994) have [O I] λ6300 smaller than this detection limit.

Nebular emission lines like Hα, [O III] $\lambda\lambda$5006, 4958 in the rest frame of the LMC were detected in the background of some of the ELHCs. We detected nebular Hα emission for ELHC 10, 12, 13, 14, 19, 21 and nebular [O III] emission for the same stars except ELHC 12 and 19. We determined the background sky as closely as possible near the star, although this was not feasible in every case due to crowding. The nebular lines of ELHC 13 originate most likely in the H II region N 120. This might be the case as well for ELHC 10, 12 and 14. ELHC 21 is located in a supernova remnant, therefore the detected forbidden nebular lines in its sky background may arise from this. ELHC 19 is not located in any obvious nebular complex.

3. Presentation of new and archive infra-red photometry

3.1. Observations and reduction of JHK data

We obtained for 18 ELHCs NIR observations on January 19 and 20, 1998 using the IRAC2b instrument mounted on the ESO-MPG 2.2 m telescope at La Silla, Chile We used the J-band, H-band and K'-band filters, in conjunction with lens A, which covers a field of $38'' \times 38''$. The detector was a 256×256 pixel NICMOS-3 array, which was read in the double-correlated readout mode. Two IR standard stars (HD 38150, F8 V, and HD 38872, A7 III; Carter & Meadows 1995) were observed during the nights in two hour intervals. The observations were done in dithering mode of 5 frames per object. The observations were reduced using dome flats. Judging from the variability of the standard stars during the run ($\Delta J^{\mathrm{inst}} = 0.05$, $\Delta H^{\mathrm{inst}} = 0.10$, $\Delta K'^{\mathrm{inst}} = 0.06$) sky conditions were reasonable. Each frame was corrected for bias and flatfielded. The sky was subtracted from each individual frame. Bad pixel masking was applied. The sources were extracted from the frames after combining the individual dithered frames. The frames were combined using the brightest star in the frame. The photometric measurements were done with aperture photometry using DAOPHOT in the MIDAS 97NOV software package. The source extraction for star ELHC 4 was done using a point spread function (PSF) fit. The achieved limiting magnitude is between 16.5^{m} for K'-band and 17.5^{m} for J-band. The detector integration times are chosen depending on the magnitude of the object.

3.2. Near infra-red colors of ELHCs

The derived NIR colors from the continuum measurements for the ELHCs are tabulated in Table 2. The table reveals that the ELHCs have quite blue NIR colors and therefore do not have strong excess emission nor is there heavy extinction by dust. The only ELHC star with NIR colors that may indicate a substantial excess emission relative to the photospheric emission is ELHC 7. Its IR colors may indicate the presence of thermal dust emission. We discuss the star further in the discussion section (Sect. 5.3). Listed in Col. 1 of Table 2 is the V-band magnitude adopted from the optical photometry dataset that was secured twelve days prior to the NIR observations. It included $BVRI$ broad band and Hα and Hα_{c} narrow band observations. This set was presented in Beaulieu et al. (2001). The photometric accuracy was at a level of 2% for stars brighter then $V = 17^{\mathrm{m}}$. We refer to that paper for details on e.g. reduction and source extraction. Compared to the low angular resolution EROS images used for the initial identification of the ELHCs, the optical broad-band images show that stars 6, 8 and 18 do not have a regular shaped PSF and could therefore consist of more than one object; indeed on the NIR images, star ELHC 18 was found to consist of two objects. It may also explain the large

Table 2. The NIR colors of the ELHC stars. The name of each ELHC is given in Col. 1. The stars indicated by an asterisk have an extra note in Sect. 3. The intrinsic $(V-J)$ colors are from Winkler (1997).

	V	$V-J$	$J-H$	$H-K'$	$(V-J)_{\rm sp.ty.}$
1	15.16	$+0.05^{\pm0.10}$	$+0.14^{\pm0.15}$	$+0.09^{\pm0.15}$	–
2	15.35	$-0.51^{\pm0.10}$	$+0.03^{\pm0.15}$	<0.13	$-0.70^{\pm0.15}$
3	15.80	$-0.39^{\pm0.10}$	$+0.16^{\pm0.10}$	$+0.23^{\pm0.15}$	$-0.57^{\pm0.13}$
4*	15.07	$-0.28^{\pm0.05}$	$+0.39^{\pm0.05}$	$-0.11^{\pm0.10}$	$-0.40^{\pm0.13}$
5*	15.75	$-0.82^{\pm0.10}$	$+0.11^{\pm0.15}$	$-0.03^{\pm0.15}$	$-0.11^{\pm0.20}$
6*	16.07	$-0.17^{\pm0.10}$	$+0.08^{\pm0.15}$	$+0.26^{\pm0.15}$	$-0.23^{\pm0.18}$
7	17.57	$-0.03^{\pm0.15}$	$+0.61^{\pm0.15}$	$+1.03^{\pm0.05}$	$-0.15^{\pm0.25}$
8*	15.74	$+0.20^{\pm0.05}$	$+0.08^{\pm0.05}$	$+0.06^{\pm0.05}$	$-0.49^{\pm0.05}$
10	13.91	$+0.49^{\pm0.05}$	$+0.15^{\pm0.05}$	$+0.13^{\pm0.05}$	$+0.43^{\pm0.10}$
12	16.08	$-0.35^{\pm0.10}$	$+0.07^{\pm0.15}$	$+0.01^{\pm0.20}$	$-0.45^{\pm0.17}$
14	15.17	$-0.38^{\pm0.05}$	$+0.04^{\pm0.10}$	$-0.05^{\pm0.10}$	$-0.62^{\pm0.03}$
15*	15.48	$+0.63^{\pm0.05}$	$+0.25^{\pm0.10}$	$-0.03^{\pm0.20}$	–
16	–	–	$+0.03^{\pm0.15}$	$-0.02^{\pm0.20}$	$-0.51^{\pm0.11}$
17	14.82	$+0.55^{\pm0.05}$	$+0.10^{\pm0.10}$	$+0.14^{\pm0.10}$	–
18*	15.77	$-0.43^{\pm0.15}$	$+0.02^{\pm0.15}$	$-0.10^{\pm0.20}$	–
19	16.01	$-0.34^{\pm0.15}$	$+0.12^{\pm0.20}$	$+0.13^{\pm0.20}$	$-0.50^{\pm0.12}$
20	15.56	$-0.42^{\pm0.15}$	$+0.07^{\pm0.20}$	<0.07	$-0.50^{\pm0.12}$
21	15.21	$-0.41^{\pm0.10}$	$+0.13^{\pm0.10}$	$+0.10^{\pm0.10}$	$-0.57^{\pm0.05}$

discrepancy found for ELHC 8 between the $(V-J)$ derived from the spectral type and the photometry. Also, in the case of ELHC 5 there exists a large difference between optical and IR magnitude, possibly revealing an extra blue source near ELHC 5. For the stars ELHC 2 and ELHC 20 only an upper limit to the K' magnitude could be established. ELHC 15 was not observed, but 2MASS measurements are available for this star.

3.3. Archive mid infra-red observations of ELHCs

In Paper I we showed that the location of the ELHCs coincides with a large 60 μm emission region in the LMC bar, as measured by IRAS. Whether the ELHCs are mid or far IR sources cannot be determined from the IRAS images that have a spatial resolution of ∼1.5 arcmin. Therefore we cross-correlated the ELHCs with higher spatial resolution archived data of the Midcourse Space Experiment (MSX) and ISO missions, obtainable from IRSA[2] and ESA[3].

In the case of the pointed observations by ISO, we find that only ELHC 21 has been observed serendipitously with ISOCAM. At 12 μm the ISO image shows no source at the location of ELHC 21 at a detection level of ∼10 mJy. ISO Observations at ∼10 μm of early type Galactic Herbig Be stars are very limited. To predict the emission based on Galactic HAeBe stars, we used the dust emission values from Galactic Herbig Ae stars at ∼10 μm from Meeus et al. (2001). Herbig Ae stars show an observed range between 3–50 Jy. In the LMC, these Ae stars would have an apparent emission at levels of 0.013–0.4 mJy. If ELHC 21 is inferred to have emission at similar levels then it would fall below the detection limit of the archived ISO image. For those Herbig Be stars for which ISO data does exist, the emission level could be ten times higher than for the Ae stars (e.g. MWC 297), but still too faint to have been detected on the available ISO image. If the ELHCs are similar to the unique and possibly pre-main sequence B2e star HD 45677, then they may show apparent flux levels at 10 μm of about 15 mJy.

With respect to MSX point source data, we find no clear correspondence between ELHCs and MSX sources. A coarse cross-correlation exists between the MSX5C G280.4587-33.3396 source that is at 25 arcsec from ELHC 2. This particular MSX point source shows also extended emission in which ELHC 2 is located. The second coarse correspondence is between ELHC 9 that is found within 20 arcsec of MSX5C G280.3695-33.4793. The IR instrument on board MSX has a sensitivity of ∼100 mJy at 8.3 μm. Assuming that the ELHCs have emission levels similar to Herbig Be stars, then ELHCs would be too faint for detection as an MSX point source.

4. The optical continuum variability of the ELHCs

The spectroscopic similarities between ELHCs and normal Be stars, combined with the lack of NIR excess described in the previous paragraphs demands a re-evaluation of the interpretation of the optical continuum variability as being due to dust (LBD and Paper I). Therefore we consider below the following two mechanisms: the previously proposed variable obscuration of the star by dust; the dust in this case should be relative cold dust, given the lack of NIR excess emission, and variable bound-free and free-free (bf-ff) continuum emission.

In the analysis we use the change in color with the brightness change (the so-called color gradient $\mathrm{d}(B-V)/\mathrm{d}V$) and the optical circumstellar color excess $E(B-V)_{\rm CS}$. The use of the optical color excess requires a precise determination of the stellar parameters. Therefore we perform this analysis only on those ELHCs that have their spectral types determined from spectra (16 out of 21), either in this paper or in LBD. We use the intrinsic color determined by Fitzgerald (1970). The color gradient (CG) for the ELHCs are determined in Paper I and LBD. They are given in the second column of Table 3. We adopt the convention that negative CGs correspond to bluer colors at fainter magnitudes. The top part of Table 3 shows that the measured negative CGs are all near the value of −0.2, whereas the positive CGs (lower part) show a considerable spread in their values.

4.1. Variable dust obscuration

The first mechanism to explain the irregular photometric variability of the ELHC stars is the obscuration of the star by dust in a stochastic way. This mechanism was proposed by LBD as the interpretation of both negative and positive CG variability. Dust obscuration naturally leads to a positive CG, where for example normal dust characterized by $R_{\rm V}=3.1$ corresponds to a CG of $\mathrm{d}(B-V)/\mathrm{d}V = 1/R_{\rm V} \simeq 0.32$. In this EROS filter

[2] From `http://irsa.ipac.caltech.edu/`

[3] From `http://www.iso.vilspa.esa.es/`

system, dust extinction causes a gradient of $d(B_E - R_E)/dR_E = 0.53$ for a $R_V = 3.3$ extinction law, as determined by Sasselov et al. (1997). The positive CG values in Table 3 show a large spread when compared to the spread in negative CGs. Stars ELHC 8, 12, 13 are compatible with variability due to dust extinction with $R_V = 3.3$. The lower values for the other ELHCs may indicate a steeper CS dust extinction law. The disappearance of the color excess at maximum brightness (Col. 4) of three stars with positive CGs (ELHC 6, 7, and 12) would support their variability due to dust obscuration.

To account for ELHCs with negative CGs as observed in 7 objects assuming variable dust obscuration, an extra source of blue radiation contributing to the observed light needs to be invoked. This source would not be obscured by the dust. Advancing the interpretation of the ELHCs as LMC HAeBe stars, scattering nebulosity near the ELHC star may function as the required blue component to explain the observed negative CGs and optical color excesses. For instance the negative color excess for ELHC 5, 16 and 20 can be explained by a star with a flattened dusty CS envelope, which is observed approximately pole-on. The scattered stellar flux by the envelope contributes significantly to the observed flux while the star undergoes little extincted. Therefore the observed color of the object is *always* bluer than the color of the underlying star itself. For an extensive discussion of the different scattering geometries and the subsequent influence on the observed color gradient we refer to LBD and Paper I. We mention here that in principle the photometric behavior of *all* the ELHC can be understood in terms of dust obscuration and a blue scattering nebula, that may or may not dominate the total observed flux.

4.2. Variable continuum bf-ff radiation

The alternative mechanism is variable continuum bf-ff radiation. It is generally observed in classical Be stars and originates in the ionized part of a flattened CS envelope (CSE, Waters et al. 1987; Dachs et al. 1988). The Be phenomenon is known to manifest itself especially towards early-type Be stars. Observationally, the Balmer emission line spectrum of the Be star is accompanied by redder photometric colors and the star appears visually brighter than their non-emission line counterparts of the same spectral type, resulting in a negative CG. Therefore the optical color excess for ELHCs with negative CGs should vanish when the star is at brightness minimum. To test this we derive in Col. 2 of Table 3 the color excess at brightness minimum for the ELHCs, again using the intrinsic color (Fitzgerald 1970) from the spectra, the 120 day light curves and the interstellar extinction towards the LMC.

Table 3 shows that of the seven stars with negative CGs, ELHC 2, 3, and 4 have a net $E(B-V)_{CS}$ at brightness minimum. This may indicate the continuing presence of an ionized CSE even at brightness minimum, if there is no additional CS dust extinction. The presence of a CSE even at brightness minimum would be corroborated by the fact that these three stars show the most variable light curves of all ELHCs, as presented in Paper I and LBD. On the other hand for the other four stars with negative CGs, the long-term photometric behavior of ELHC 5, 16 and 20 displays an occasional brightness "bump" (ELHC 5 and 16) or a rather slow brightness change (ELHC 20). For these three stars we are most likely observing the underlying photosphere, which is corroborated by the small negative $E(B-V)_{CS}$ derived in Table 3. Negative values of $E(B-V)_{CS}$ are not uncommon for Galactic classical Be stars (see Fig. 1 of Waters et al. 1987). The negative value found for ELHC 5 is extreme. Finally, the color excess of ELHC 11 is unreliable, given that the object is only partially resolved.

Table 3. Color gradients and optical color excess for the ELHCs with spectra available. The color excess is derived at minimum and maximum light. If the ELHC variability is due to variable bf-ff emission the $E(B-V)_{CS}$ vanishes at minimum light. On the other hand $E(B-V)_{CS}$ is expected to vanish at maximum light if the variability is due to variable dust obscuration (see text).

	$d(B_E - R_E)/dR_E$ CG	$E(B-V)_{CS}$ brightness min.	$E(B-V)_{CS}$ brightness max.
2	$-0.32^{\pm0.03}$	$+0.08^{\pm0.04}$	$+0.23^{\pm0.04}$
3	$-0.14^{\pm0.03}$	$+0.09^{\pm0.04}$	$+0.14^{\pm0.04}$
4	$-0.22^{\pm0.05}$	$+0.10^{\pm0.07}$	$+0.18^{\pm0.07}$
5	$-0.26^{\pm0.04}$	$-0.11^{\pm0.05}$	$-0.05^{\pm0.05}$
11[1]	$-0.24^{\pm0.04}$	$+0.22^{\pm0.03}$	$+0.27^{\pm0.03}$
16	$-0.24^{\pm0.04}$	$-0.05^{\pm0.05}$	$-0.02^{\pm0.03}$
20	$-0.27^{\pm0.04}$	$-0.08^{\pm0.06}$	$-0.05^{\pm0.03}$
6	$+0.07^{\pm0.03}$	$+0.10^{\pm0.05}$	$+0.03^{\pm0.05}$
7	$+0.07^{\pm0.03}$	$+0.10^{\pm0.06}$	$+0.00^{\pm0.06}$
8	$+0.66^{\pm0.15}$	$+0.16^{\pm0.04}$	$+0.11^{\pm0.04}$
12	$+0.58^{\pm0.10}$	$+0.13^{\pm0.07}$	$+0.05^{\pm0.07}$
13	$+0.45^{\pm0.11}$	$+0.26^{\pm0.04}$	$+0.19^{\pm0.04}$
14	$+0.11^{\pm0.04}$	$+0.18^{\pm0.03}$	$+0.13^{\pm0.03}$
19	$+0.37^{\pm0.06}$	$+0.14^{\pm0.03}$	$+0.10^{\pm0.03}$
21	$-0.03^{\pm0.05}$	$+0.13^{\pm0.04}$	$+0.12^{\pm0.04}$

[1] Object is partially resolved (Sect. 2).

As the ionized CSE produces both the emission line spectrum and the optical color excess of the classical Be stars, these two quantities are related. An approximate relation between $E(B-V)_{CS}$ and the EW of the Hα line for Galactic Be stars was derived by Dachs et al. (1988), which is shown in Fig. 4 together with the Hα emission and CS color excess of the ELHCs. The filled asterisks indicate the *simultaneous* measurement of the two quantities, derived from narrow band Hα and Hα_{cont} and broad band *BVRI* imaging (for details see Beaulieu et al. 2001). The circles represent the color excess derived from the EROS light curve of the stars: filled circles indicate brightness minima, open circles indicate brightness maxima. The two dashed-dotted lines indicate the range of values found by Dachs et al. (1988). Figure 4 indicates that the ELHCs with marginal Hα emission have marginal color excess, as expected for stars surrounded by an ionized CSE. ELHC 11 shows a dramatic decrease in color excess from the higher angular resolution broad band imaging (asterisks) when compared to the EROS measurements (circles). It was also found

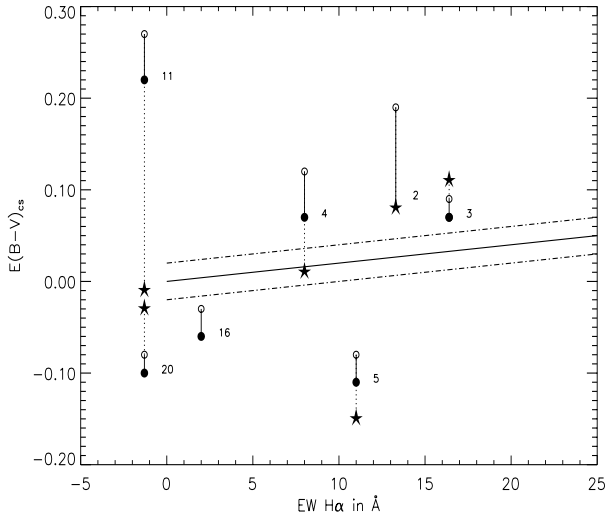

Fig. 4. The relation between Hα equivalent width and $E(B-V)_{\rm CS}$ for ELHCs that have negative color gradients, i.e. bluer color at brightness minimum. The stars in the figure include objects discussed by LBD for which spectral information is available. The filled asterisks are measurements taken simultaneously. The circles indicate the range in $E(B-V)_{\rm CS}$ derived from the EROS light curves. The filled circle is the EROS color excess at brightness minimum. The full line is the approximate relation for Galactic Be stars derived by Dachs et al. (1988), the adjacent dashed-dotted lines indicate the observed range of values.

in the analysis of the spectra (Sect. 2.3) that ELHC 11 has a very close-by F-type companion. Note the strong difference in EW(Hα) for ELHC 2 as determined in LBD (104 Å) and the one determined here from narrow band photometry (13 Å). As discussed in LBD, ELHC 2 is located inside the bright H II region N 120. The strong nebular emission hampers a good determination of the EW of the line.

We thus see that the ELHCs with a negative CG (bluer-when-fainter) can be understood in terms of a stellar component and a variable CSE component, as far as the correlations between the optical color excess, the Hα emission, the CG and the corresponding photometric variability is concerned. The mechanism is therefore a strong alternative for stars with negative CGs. The star ELHC 5 could be an exception to this.

5. Discussion: The nature of the ELHCs

We have presented in this paper low resolution spectra and near IR photometry of candidate HAeBe stars in the LMC, the so-called ELHCs. These stars were presented for the first time in LBD and in Paper I. They were selected on the basis of their peculiar photometric variability, thought to be due to variable dust obscuration. The low resolution spectra presented here indicate that the stars are nearly all spectral type B, with one exception. The NIR observations reveal that the ELHCs do not have strong excess emission in the JHK' bands (except one), therefore probably lacking warm dust in their circumstellar environment.

5.1. The absence of CS NIR emission

The NIR properties of Galactic HAeBe stars are easily distinguished from the properties of classical Be stars. The ionized CSE of classical Be stars causes a minor excess (e.g. Johnson 1967; Dachs et al. 1988; Dougherty et al. 1994) in the NIR passbands. It displays a power-law spectrum that decreases with increasing wavelength. On the other hand, the NIR excess emission of HAeBe stars is generally found to be much stronger and is thought to be caused by small hot dust grains. Their NIR spectra show a striking similarity from 2 to 7 μm (Meeus et al. 2001). Only a few HAeBe stars do not have dust emission (i.e. the group III objects of Hillenbrand et al. 1992). Although these stars were selected by Hillenbrand et al. because they are associated with star forming regions, only BD +65 1637, B2/3e and HD 53367, B0e of the 6 group III stars are still considered to be genuine HAeBe stars, primarily because of IR considerations (e.g. Van den Ancker et al. 1998). The lack of strong thermal dust emission of the ELHCs argues against a PMS nature for the stars.

The exact influence of metallicity on CS dust is difficult to predict, but some observations indicate that a dependency does exist. The well-known B[e] supergiants in the Magellanic Clouds follow the trend of having smaller NIR excess in the Small Magellanic Cloud (SMC) than in the LMC. Also the amount of extinction per unit H I column density is a factor 10 lower in the SMC than in the Galaxy (Bouchet et al. 1985). In de Wit et al. (2003) we tried to estimate the influence of metallicity on the CS dust of HAeBe stars for the case of the SMC, by simply scaling the observed dust emission of Galactic HAeBe stars to the SMC metallicity. Here we follow the same procedure with the difference of scaling the dust emission to LMC metallicity (one third solar, Russell & Dopita 1990). The result is presented in Fig. 5. The figure shows the *NIR* colors of Galactic HAeBe stars as filled symbols, if they would be LMC HAeBe stars. The measured (unscaled) *JHK* colors are given as open symbols (from Hillenbrand et al. 1992). The location of classical Be stars is indicated by the hatched area (Dougherty et al. 1994). The figure leads to the conclusion that in contrast to the SMC case, dust emission could still be substantial at the metallicity of the LMC.

In Fig. 6, we show the same color–color diagram with the ELHCs presented by open asterisks (bluer-when-fainter) and filled asterisks (redder-when-fainter). The Main Sequence is the full line from Koornneef (1982). The figure shows that all ELHCs have minor NIR excesses (if any), with ELHC 7 as an exception. Note that there is hardly any difference between the distribution of the two ELHC variability groups. The open circles are the metallicity-scaled Galactic Herbig Be stars (the filled asterisks of Fig. 5). The hatched area again indicates the location of classical Be stars. The location of the ELHCs in the diagram suggests that the NIR excess is compatible with bf-ff emission excesses.

A further reduction of the CS dust content could be caused by the higher ambient UV radiation field at lower metallicities. A high UV radiation field is also found in young massive Galactic clusters. The percentage of dusty disks in the massive 2 Myr Galactic cluster NGC 6611 is found to be very low

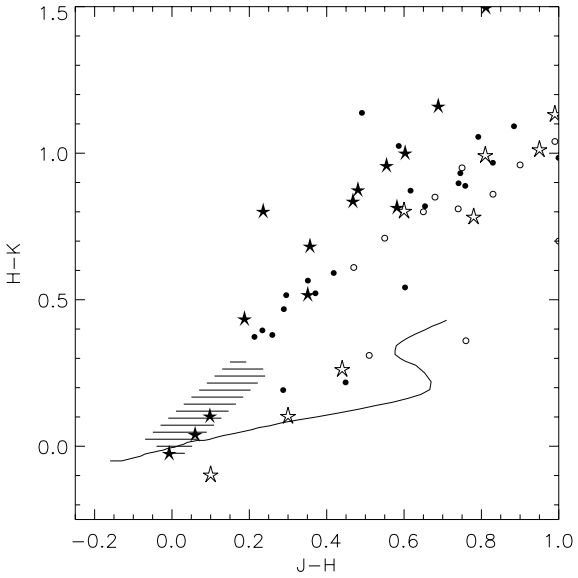

Fig. 5. The color–color diagram shows the change in NIR excess of Galactic HAeBe stars (open symbols), if they were PMS stars with LMC metal abundance (filled symbols). Asterisks are used for Herbig Be stars and circles for the Herbig Ae stars (derived from data by Hillenbrand et al. 1992). The full line indicates the Main Sequence from Koornneef (1983) and the hatched area the region occupied by the sample of Classical Be stars from Dougherty et al. (1994).

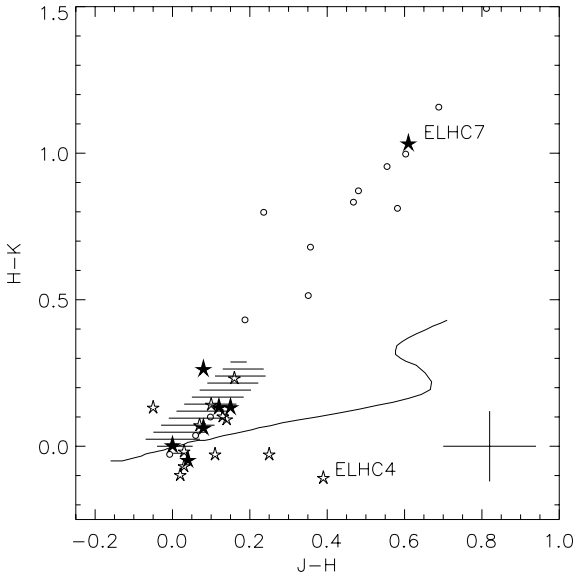

Fig. 6. The observed NIR colors for the majority of the ELHCs (see Table 2). The ELHCs are represented by the filled asterisks (redder-when-fainter) and open asterisks (bluer-when-fainter). The full line is the Main Sequence from Koornneef (1983). The hatched area indicates the region where the Galactic classical Be stars are located, adopted from Dougherty et al. (1994). The only star with appreciable excess is star ELHC 7. For comparison, the open circles are the metallicity-scaled NIR colors of Galactic Herbig Be stars of Fig. 5. Average error bar is given in the right bottom.

(Hillenbrand et al. 1993). They found that some 90% (27/30) of the PMS emission line members have optical and IR properties similar to classical Be stars. This argues for short dust disk dispersal times in a cluster environment containing massive stars, where possibly stellar encounters and/or UV irradiation can play a role. Progressively metal poor galaxies may therefore show fewer stars having thermal CS dust emission, due to the increased UV interstellar radiation field. Optical and NIR characteristics of classical Be stars may be common to intermediate mass PMS stars at lower metallicity.

5.2. Variability due to dust or ionized gas?

In Sect. 2.4 we showed that the Balmer decrements are practically the same for Galactic Herbig Be stars, classical Be stars and ELHCs. This indicates a similar state of the ionized CS environment, and that the Balmer decrement does not help to discriminate between the different types of star. Other optical properties, like $E(B-V)_{\rm CS}$ and color–brightness behavior, were interpreted in terms of two different mechanisms causing photometric variability, i.e. due to bf-ff continuum emission or due to dust obscuration. These two variability mechanisms predict opposite behavior of the color as a function of brightness. The ELHCs show both type of behavior and we therefore discussed the ELHCs accordingly: (I) bluer-when-fainter (11 objects); (II) redder-when-fainter or grey (9 objects). Only one object shows grey variability.

Type I: The bluer-when-fainter stars: we can list five arguments in favor of variable bf-ff continuum radiation as the dominant mechanism causing the variability of type I ELHCs: (1) the color gradient; (2) the optical color excess; (3) the color variability; (4) the correlation with Hα emission; (5) the convergence of the color gradient to a value of –0.24. For the alternative dust-obscuration/scattering-nebula model (see LBD) the color gradient depends on the grain size of the obscuring cloud, the size of the scattering nebula and the scattering function of its constituents, and may be expected to have a range of values. Supporting this interpretation is the small NIR excess of the stars, similar to the classical Be stars. The NIR emission is less than expected from first order dust scaling arguments. In addition, the early type classical Be stars are known to exhibit the largest brightness variability (Hubert & Floquet 1998); the ELHCs with a bluer-when-fainter behavior are all early B type, except ELHC 5. The proposed interpretation here is in contrast with the one presented in LBD and Paper I, where the ELHCs were inferred to be surrounded by unresolved blue reflection nebulae. It seems more attractive for these stars to adopt the simplest (least parameter) model: the classical Be model. The argument against this interpretation is the observed variability time scale of 20–30 days, which is uncommon among the classical Be stars. However a large variety of time scales and light curve types of ~1300 blue variable stars in the LMC have recently been presented by Keller et al. (2002), claiming that the ELHC-type of photometric variability is quite common in the LMC.

Type II: The redder-when-fainter stars: the ELHCs of type II display a variability that is different from variable bf-ff emission. That the variability is due to variable dust

obscuration cannot be excluded. We have seen that the color gradient of some stars is compatible with obscuration by normal dust. This predicts that ELHCs of type II are mid and/or far IR sources and therefore warrant follow-up Spitzer observations. Alternative interpretations to the one proposed here are variability due to unstable pulsation modes or stellar spots. Periodic instabilities in Be star photospheres have however observed time scales of the order of a day (e.g. Balona 1995), much shorter than the ELHC time scale. Large stellar spots may exist on the surface of Herbig Be stars, inferred from the X-ray activity of MWC 279 (Hamaguchi et al. 2002). However also in this case one expects time scales of the order of 1 day, modulated by the star's rotational period. With respect to star formation indicators in the field, ELHCs of type II are preferentially located around the HII complex N 120. Also the spectrum of ELHC 19 revealed nebular emission and possibly evidence for outflow activity. Therefore it seems that ELHCs of type II are best interpreted as pre-main sequence Be type stars, but high resolution mid- and far-IR observations are strongly needed to confirm this.

Despite two different mechanisms explaining the color–magnitude variability for the type I and II ELHC stars, the brightness variability *as function of time* can be quite similar. For instance ELHC 4 (type I) and ELHC 8 (type II) show a similar constant brightness decrease for 40 days (see the light curves presented in LBD and Paper I), followed by a sudden increase to the original flux level in about 10 days. The same applies to ELHC 2 (I), 13 and 14 (both II), stars that show a quasi-regular brightness variability. We see thus that different variability mechanisms can cause similar brightness changes on similar time scales. Making a similar inventory of the variability displayed by Galactic Herbig Be stars based on the light curves presented by Herbst & Shevchencko (1999), we see that both variability types occur (see Appendix A) and thus that both variability mechanisms may be at play among early type Galactic PMS stars as well. The much larger light curve database of Magellanic Cloud early type stars presented by Keller et al. (2002) and Mennickent et al. (2002) could shed more light on the mechanisms causing the various types of light curve and the corresponding color–magnitude behavior of pre-main sequence and classical Be type stars.

5.3. A confirmed HAeBe star: ELHC 7

The near IR observation presented in Sect. 3 revealed that the only star with NIR excess is ELHC 7, and is therefore the strongest candidate PMS star in our sample of Magellanic Cloud HAeBe stars. ELHC 7 was reported in LBD to have the largest amplitude variation over a time span of 150 days. The stars' behavior over the much longer period of 3 years is shown in Fig. 7, as observed by the MACHO collaboration. The full 7.5 year MACHO light curve can be obtained from `http://wwwmacho.anu.edu.au/` (MACHO star 79.5862.453). ELHC 7 exhibits continuously variable brightness decreases with a maximum amplitude of $\Delta R \simeq 0.9^{\rm m}$ (in the MACHO broad band *R*-filter) over 3 years of the

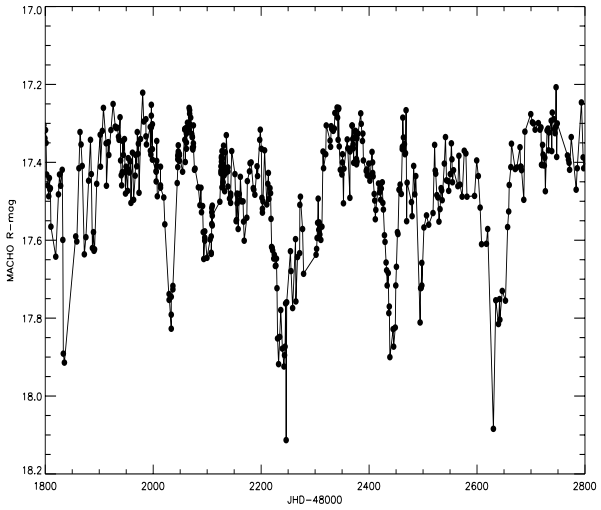

Fig. 7. Part of the available 7.5 year light curve of ELHC 7 in the broadband MACHO *R*-filter, obtained by the MACHO collaboration. Average error on a measurement is $0.05^{\rm m}$.

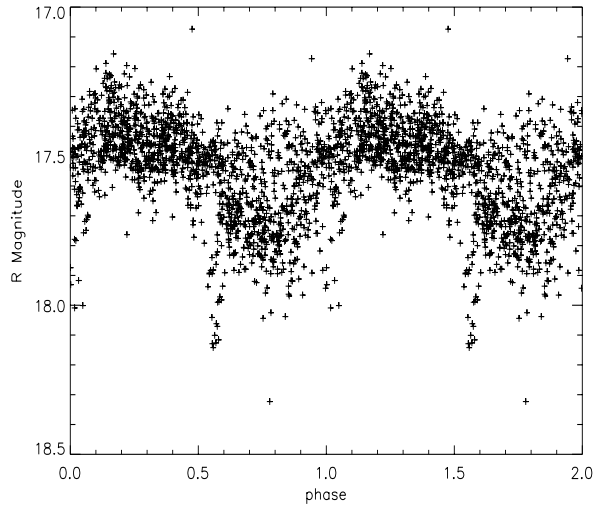

Fig. 8. The MACHO 7.5 year light curve of ELHC 7 folded on the most probable period of 191.3 days. The folded light curve has been plotted twice.

observations. The full MACHO light curve reveals a quasi-periodicity around a period of 190 days. The folded light curve on this period is shown in Fig. 8 and reveals that (1) ELHC 7 laps minima (2) the range of measurements at a certain phase ($\sim 0.25^{\rm m}$) is larger than the error bars on the individual measurements, $\sigma(R) \simeq 0.05$. The color variability of the stars is redder-when-fainter, where the scatter in the color becomes large during the deepest minima. The amplitude of variability displayed by ELHC 7 is less than the "Algol-type" minima exhibited by the Galactic PMS UX Orionis subgroup, however the variability on a time scale of tens of days and the tendency to display a sudden decrease in brightness and a subsequent recovery to the original flux level is quite similar (e.g. Bibo & Thé 1991). Moreover it is suspected that the UX Ori type of variability might be cyclic, where for example UX Ori has a probable period of around 319 days. ELHC 7 seems to be very similar to the UX Ori type stars.

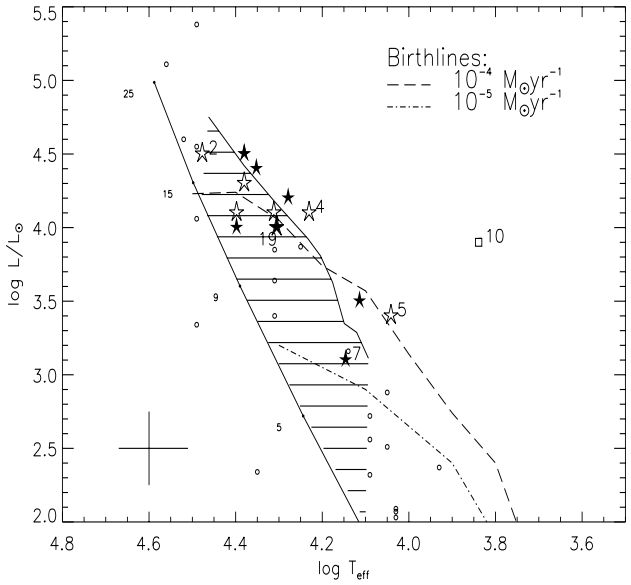

Fig. 9. The HRD for the ELHCs, derived from spectroscopy. The type I ELHCs are given by the open asterisks, the type II by the filled asterisks. The Main Sequence is indicated by the full line, with ZAMS masses indicated. Classical Be stars are expected in the hatched area. Also indicated are two birthlines of Palla & Stahler (1992) for different mass accretion rates. Note that ELHC 7 is compatible with the Galactic mass accretion rate of $10^{-5}\,M_{\odot}\,\mathrm{yr}^{-1}$. The small open dots are Galactic HAeBe stars taken from Testi et al. (1998). The open square is the F supergiant ELHC 10 and is close to the classical instability strip.

5.4. The HR-diagram

In our previous studies, we have put forward the suggestion that the position of the ELHCs in the HR-diagram indicates that at lower metallicity the proto-stellar mass accretion rate could be higher, provided that ELHCs are PMS stars. In de Wit et al. (2003) the location of an UX Ori type star in the Small Magellanic Cloud would support the notion of a higher mass accretion rate at lower metallicities.

The mass accretion rate is determined from the stellar parameters relative to the Palla & Stahler (1993) birthlines for different accretion rates. In Fig. 9 we present the ELHC stellar parameters derived from spectroscopy in an HR-diagram. Following the previous sections we distinguish between type I ELHCs (open asterisks) and type II (filled asterisks). Given the previous discussion on the variability of the stars we derived the stellar parameters for type I ELHCs at brightness minimum, and for type II ELHCs at brightness maximum. We adopted the spectral type to temperature calibration and bolometric correction from Schmidt-Kaler (1982). The LMC distance modulus was taken to be 18.5 (see Walker 1999).

The HR-diagram in Fig. 9 shows the Zero Age Main Sequence by the full line. The hatched area corresponds to the expected location of classical Be stars, when their luminosity is derived from their absolute visual magnitude as given by Zorec & Briot (1997). In addition, two luminosity upper limits (birthlines) for PMS stars from Palla & Stahler (1993) are indicated, corresponding to the canonical Galactic mass accretion rate of $10^{-5}\,M_{\odot}\,\mathrm{yr}^{-1}$ (dashed-dotted) and $10^{-4}\,M_{\odot}\,\mathrm{yr}^{-1}$ (dashed). We see that:

(1) the confirmed HAeBe star ELHC 7 is one of the least luminous stars in our sample; the object is compatible with the *Galactic* mass accretion rate of $10^{-5}\,M_{\odot}\,\mathrm{yr}^{-1}$;
(2) no apparent difference in stellar parameters exists between type I and II ELHCs;
(3) the stellar parameters of the type I ELHCs are compatible with the expected parameters of classical Be stars, except the peculiar object ELHC 5;
(4) the luminosity of some of the type II ELHCs are in excess of the $10^{-4}\,M_{\odot}\,\mathrm{yr}^{-1}$ birthline, and would indicate even higher mass accretion rates. It is noteworthy that some Galactic HAeBe stars (small open circles) have similar stellar parameters.

6. Conclusions

We have found that the proposed LMC PMS stars are nearly all emission line stars of B-type that lack substantial thermal dust emission in the NIR. The optical continuum variability for half of the sample is better interpreted as variable bf-ff gas emission. These characteristics do not a priori exclude that the stars are in a PMS phase, given that the type of optical variability is also observed among Galactic HAeBe stars, and that a low metallicity environment may reduce the total CS dust emission. However for the case of PMS stars at LMC metallicity, first order dust scaling shows that one may still expect substantial CS dust emission. Therefore it seems very unlikely that this half of the ELHC sample is in a pre-main sequence phase. The other half of the sample could reveal CS dust emission in the mid or far IR, based on the type of optical variability. These ELHCs may therefore be stars in a PMS stage, although it is not known whether rapidly rotating Be stars display a similar type of optical variability.

The star ELHC 7 is the only star in our sample of proposed LMC PMS stars that has thermal dust emission in the NIR. This star seems to be an LMC counterpart of the Galactic PMS UXOri stars. Its stellar parameters indicate that its proto-stellar mass accretion rate is not different from the canonical Galactic rate of $10^{-5}\,M_{\odot}\,\mathrm{yr}^{-1}$.

Acknowledgements. W.J.d.W. would like to thank the Institut d'Astrophysique de Paris where most of the work was done for their hospitality. Dr J. Vink is acknowledged for critically reading the manuscript. This publication makes use of data products from the Two Micron All Sky Survey, which is a joint project of the University of Massachusetts and the Infra-red Processing and Analysis Center/California Institute of Technology, funded by the National Aeronautics and Space Administration and the National Science Foundation. This paper utilizes public domain data originally obtained by the MACHO Project, whose work was performed under the joint auspices of the US Department of Energy, National Nuclear Security Administration by the University of California, Lawrence Livermore National Laboratory under contract No. W-7405-Eng-48, the National Science Foundation through the Center for Particle Astrophysics of the University of California under cooperative agreement AST-8809616, and the Mount Stromlo and Siding

Spring Observatory, part of the Australian National University. Lastly, we wish to thank the referee, C. Grady, for valuable suggestions that significantly improved the manuscript.

Appendix A: Color gradients of Galactic HAeBe stars

We present here the fits to the color–brightness behavior of Galactic HAeBe stars. We used the database of Herbst & Shevchenko (1999)[4]. We selected the stars on their B-spectral type and on available accurate measurements. The measurements of some Herbig Be stars in the database have large scatter. Some selected stars presented here also show scattered measurements (e.g. MWC 297). To increase visibility we binned the data in magnitude intervals of 0.01. Only magnitude bins which contain three or more measurements were taken into account in the weighed fit of the color gradient $\mathrm{d}(B-V)/\mathrm{d}V$. The weights of each fit are the standard deviations of the calculated (unweighed) mean in each bin. The panels are ordered according to increasing color gradient. The last two panels (V 1686 Cyg and LkHα 234) show a possible color reversal (the scattering is quite large). For these two stars we have fitted only the least scattered measurements, which correspond to the redder-when-fainter part. The measurements are given in Table A.1.

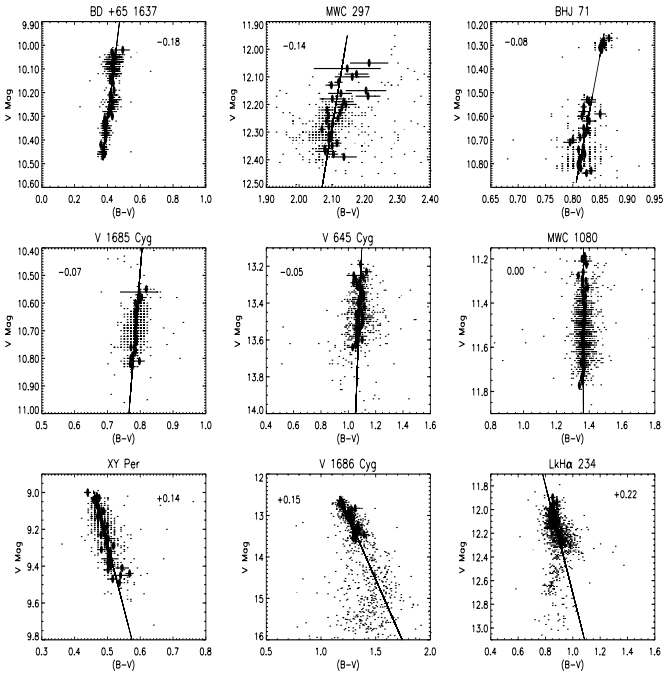

Fig. A.1. Fits to the observed color–magnitude slopes of Galactic HAeBe stars. The 9 stars are of spectral type B. The data forms the basis of HAeBe variability analysis of Herbst & Shevchenko (1999). Each panel shows $(B-V)$ color against V-magnitude of each the complete dataset (small dots) and the averaged measurement per magnitude bin (filled dots).

[4] From `http://www.astro.wesleyan.edu/`

Table A.1. The determined color gradients and color excess for Galactic Herbig Be stars.

Star	Spectral type	$\mathrm{d}(B-V)/\mathrm{d}V$	$E(B-V)$
BD 65d1637	B2/3	-0.18 ± 0.02	0.66
MWC 297	O9/B1.5	-0.14 ± 0.04	2.42
BHJ 71	B0/8	-0.08 ± 0.01	1.06
V 1685 Cyg	B2	-0.07 ± 0.01	1.05
V 645 Cyg	O7	-0.05 ± 0.02	1.42
MWC 1080	B0	$+0.00 \pm 0.01$	1.66
XY Per	B6	$+0.14 \pm 0.01$	0.59
V 1686 Cyg	B2/5	$+0.15 \pm 0.01$	1.35
LkHα 234	B3/7	$+0.22 \pm 0.02$	0.99

References

Aubourg, E., Bareyre, P., Brehin, S., et al. 1993, Nature, 365, 623
Balona, L. A. 1995, MNRAS, 277, 1547
Beaulieu, J.-P., de Wit, W. J., Lamers, H. J. G. L. M., et al. 2001, A&A, 380, 168
Beaulieu, J. P., Lamers, H. J. G. L. M., Grison, P., et al. 1996, Science, 272, 995
Bibo, E. A., & Thé, P. S. 1991, A&AS, 89, 319
Boehm, T., & Catala, C. 1994, A&A, 290, 167
Boehm, T., & Hirth, G. A. 1997, A&A, 324, 177
Bouchet, P., Lequeux, J., Maurice, E., Prevot, L., & Prevot-Burnichon, M. L. 1985, A&A, 149, 330
Brandner, W., Grebel, E. K., Barbá, R. H., Walborn, N. R., & Moneti, A. 2001, AJ, 122, 858
Carter, B. S., & Meadows, V. S. 1995, MNRAS, 276, 734
Dachs, J., Kiehling, R., & Engels, D. 1988, A&A, 194, 167
Dachs, J., Rohe, D., & Loose, A. S. 1990, A&A, 238, 227
de Wit, W. J. 2001, Ph.D. Thesis, University of Utrecht
de Wit, W. J., Beaulieu, J. P., & Lamers, H. J. G. L. M. 2002, A&A, 395, 829
de Wit, W. J., Beaulieu, J.-P., Lamers, H. J. G. L. M., Lesquoy, E., & Marquette, J.-B. 2003, A&A, 410, 199
Didelon, P. 1982, A&AS, 50, 199
Dougherty, S. M., Waters, L. B. F. M., Burki, G., et al. 1994, A&A, 290, 609
Finkenzeller, U., & Mundt, R. 1984, A&AS, 55, 109
Fitzgerald, M. P. 1970, A&A, 4, 234
Hamaguchi, K., Terada, H., Bamba, A., & Koyama, K. 2000, ApJ, 532, 1111
Hamann, F., & Persson, S. E. 1992, ApJS, 82, 285
Hanuschik, R. W., Hummel, W., Dietle, O., & Sutorius, E. 1995, A&A, 300, 163
Hanuschik, R. W., Hummel, W., Sutorius, E., Dietle, O., & Thimm, G. 1996, A&AS, 116, 309
Herbst, W., & Shevchenko, V. S. 1999, AJ, 118, 1043
Hernández, J., Calvet, N., Briceño, C., Hartmann, L., & Berlind, P. 2004, AJ, 127, 1682
Hillenbrand, L. A., Massey, P., Strom, S. E., & Merrill, K. M. 1993, AJ, 106, 1906
Hillenbrand, L. A., Strom, S. E., Vrba, F. J., & Keene, J. 1992, ApJ, 397, 613
Hubeny, I., Lanz, T., & Jeffery, C. S. 1994, TLUSTY and SYNSPEC: A Users's Guide, Newsletter on Analysis of Astronomical Spectra, Univ. of St. Andrews
Hubert, A. M., & Floquet, M. 1998, A&A, 335, 565
Hunter, D. 1997, PASP, 109, 937
Jacoby, G. H., Hunter, D. A., & Christian, C. A. 1984, ApJS, 56, 257

Johnson, H. L. 1967, ApJ, 150, L39
Keller, S. C., Bessell, M. S., Cook, K. H., Geha, M., & Syphers, D. 2002, AJ, 124, 2039
Koornneef, J. 1983, A&A, 128, 84
Lamers, H. J. G. L. M., Beaulieu, J. P., & De Wit, W. J. 1999, A&A, 341, 827
Laval, A., Rosado, M., Boulesteix, J., et al. 1992, A&A, 253, 213
Malyuto, V., & Schmidt-Kaler, T. 1997, A&A, 325, 693
Meeus, G., Waters, L. B. F. M., Bouwman, J., et al. 2001, A&A, 365, 476
Mennickent, R. E., Pietrzyński, G., Gieren, W., & Szewczyk, O. 2002, A&A, 393, 887
Okazaki, A. T. 1991, PASJ, 43, 75
Palla, F., & Stahler, S. W. 1993, ApJ, 418, 414
Panagia, N., Romaniello, M., Scuderi, S., & Kirshner, R. P. 2000, ApJ, 539, 197
Romaniello, M., Robberto, M., & Panagia, N. 2004 [arXiv:astro-ph/0402459]
Russell, S. C., & Dopita, M. A. 1990, ApJS, 74, 93
Sasselov, D. D., Beaulieu, J. P., Renault, C., et al. 1997, A&A, 324, 471
Schmidt-Kaler, T. 1982, in Landolt Bornstein Vol. 2, Sub-vol. B (Berlin: Spinger Verlag)
Slettebak, A. 1949, ApJ, 110, 498
Testi, L., Palla, F., & Natta, A. 1998, A&AS, 133, 81
Štefl, S., Baade, D., Rivinius, T., et al. 2003, A&A, 402, 253
Van den Ancker, M. E., De Winter, D., & Tjin A Djie, H. R. E. 1998, A&A, 330, 145
Vieira, S. L. A., Corradi, W. J. B., Alencar, S. H. P., et al. 2003, AJ, 126, 2971
Walker, A. 1999, in Post-Hipparcos cosmic candles, ed. A. Heck, & F. Caputo (Astrophysics and space science library), 237, 125
Waters, L. B. F. M., Cote, J., & Lamers, H. J. G. L. M. 1987, A&A, 185, 206
Waters, L. B. F. M., & Waelkens, C. 1998, ARA&A, 36, 233
Winkler, H. 1997, MNRAS, 287, 481
Zorec, J., & Briot, D. 1997, A&A, 318, 443